Sensors and Materials, Vol. 21, No. 8 (2009) 433–444
MYU Tokyo

S & M 0782

Fabrication of $Au_{core}Co_3O_{4shell}$/PAA/HRP Composite Film for Direct Electrochemistry and Hydrogen Peroxide Sensor Applications

Xiaohua Chen[1], Huan Guo[1], Jing Yi[1,2] and Jianqiang Hu[1,*]

[1]Department of Chemistry, College of Chemistry and Chemical Engineering, South China University of Technology, Guangzhou 510640, P. R. China
[2]School of Chemistry and Environment, South China Normal University, Guangzhou 510640, P. R. China

(Received January 16, 2009; accepted July 10, 2009)

Key words: biosensor, nanomaterial, polyacrylic acid, hydrogen peroxide, direct electrochemistry

A completely new biosensor composed of cube-shaped $Au_{core}Co_3O_{4shell}$ nanoparticles ($Au_{core}Co_3O_{4shell}$), polyacrylic acid (PAA), and horseradish peroxidase (HRP) modified film electrode was fabricated for the first time. The biocompatibility and electrochemical properties of the resulting $Au_{core}Co_3O_{4shell}$-PAA-HRP composite film were studied by electrochemical impedance spectroscopy, UV-visible spectroscopy, and cyclic voltammetry. The UV-vis spectrum obtained suggests that HRP retains its native conformation in the modified film. The immobilized HRP shows a pair of quasi-reversible redox peaks at −0.31 V in 20 mM PBS (pH 7.0), and the biosensor shows a fast amperometric response to hydrogen peroxide with a linear range of 2.0×10^{-6} to 3.7×10^{-4} M. The kinetic parameters such as k_s (electron transfer rate constant) and K_M (Michaelis-Menten constant) are evaluated to be about 7.4 s^{-1} and 0.91 mM, respectively. These indicate that the cube-shaped $Au_{core}Co_3O_{4shell}$ nanoparticles are an ideal candidate material for direct electrochemistry of redox proteins and for the construction of related enzyme biosensors, and that they may find potential applications to biomedical, food, and environmental analyses and detection.

1. Introduction

Recently, nanomaterial-constructed biosensors have been attracting extensive interest because nanomaterials not only effectively retain the bioactivity of enzymes trapped in the biosensor but greatly facilitate the direct electron transfer between the enzyme and the electrode.(1) Excellent biocompatibility, stability, and sensitivity are crucial for biosensors to offer effective electron transfer channels between the redox-

*Corresponding author: e-mail: jqhusc@scut.edu.cn

active enzyme and the electrode.[2] To improve these electrochemical properties, many studies have been conducted using different nanomaterials because the electrochemical properties of biosensors are associated with the component, structure, size, and shape of nanomaterials.[3–7] For example, Dai *et al.* reported that a biosensor fabricated using tetragonal pyramid-shaped porous ZnO nanostructures has better biosensing properties than that fabricated using solid spherical ZnO nanoparticles.[4] Among nanomaterials, composite nanostructures usually exhibit better electrochemical properties than nanostructures possessing a single component because one dopant component amplifies the electrochemical properties of the other component.[8,9] Ivnitski *et al.* integrated biologically derived silica with single-walled carbon nanotubes to fabricate a biosensing platform with excellent film-forming ability, good adhesion, biocompatibility, and bioelectrocatalytic properties.[5]

Cobalt tetroxide (Co_3O_4) is a spinel-type compound of 3*d* transition-metal oxides,[10] whose nanostructures show unique electronic and chemical properties and are widely applied in electrochemistry,[11] magnet,[12] and catalysis areas.[13] Currently, there is a broad research interest in the preparation of Co_3O_4 with novel shapes and composite structures, such as nanotubes,[14] nanoboxes,[15] nanocubes,[16] nanohydrotalcites,[17] Co_3O_4/Fe_2O_3,[18] Co_3O_4/Si,[19] and Co_3O_4/ZnO.[20] We have synthesized $Au_{core}Co_3O_{4shell}$ composite nanocubes, and demonstrated that they have better electrochemical performance than pure Co_3O_4 nanocubes.[9] However, to the best of our knowledge, newly shaped or composite Co_3O_4 nanomaterials are rarely used to construct biosensors, although biosensors based on Co_3O_4 nanoparticles have been fabricated. For example, layered Co_3O_4 nanoflakes with spongy nanostructure have been utilized to fabricate a hydrogen peroxide biosensor with high bioelectrocatalytic activity.[21]

Many researchers have been attempting to introduce inorganic nanomaterials and biomaterials into organic polymer matrices because forming ordered structures can better retain the bioactivity of biomaterials and enhance the properties of the composite materials.[22,23] Additionally, compared with other kinds of media, one advantage in the use of organic polymers is that inorganic nanoparticles can be introduced easily into the matrix under mild conditions, and their flexibility and functional groups can provide a favorable microenvironment for redox proteins to realize direct electrochemistry and biomimetics.[24–26] Among organic polymers, polyacrylic acid (PAA) as a water-soluble biocompatible polymer has good dispersing ability for and biocompatibility with water-soluble nanomaterials and enzymes, which has been used in biosensor fabrication and direct electrochemical studies.[27,28]

In this study, we report a completely new biosensor composed of $Au_{core}Co_3O_{4shell}$ nanocubes ($Au_{core}Co_3O_{4shell}$), PAA, and a horseradish peroxidase (HRP)-modified film electrode. The biocompatibility and electrochemical properties of the $Au_{core}Co_3O_{4shell}$-PAA-HRP composite film were studied by electrochemical impedance spectroscopy (EIS), UV-visible spectroscopy (UV-vis), and cyclic voltammetry (CV).

2. Materials and Methods

2.1 *Materials*

HPR (> 250 u/mg) was purchased from Yuanju Biology Science and Technology Co., Ltd. (Shanghai, China). PAA (average degree of polymerization, 800±100; CAS No., 9007-20-9) was purchased from Kemiou Chemical Reagent Co., Ltd. (Tianjin, China). The other chemical reagents used such as hydrogen peroxide, sodium dihydrogen phosphate, disodium hydrogen phosphate, potassium chloride (KCl), potassium ferricyanide ($K_3[Fe(CN)_6]$), potassium ferrocyanide ($K_4[Fe(CN)_6]$), concentrated hydrochloric acid, concentrated nitric acid, and highly pure nitrogen gas were obtained from Tianjin Chemical Reagent Co. (Tianjin, China). All the above reagents were analytical grade and used without further purification. All aqueous solutions were prepared with Milli-Q purified water (> 18.0 MΩ cm). All samples for electrochemical measurements were prepared with pH 7.0 phosphate-buffered solution (PBS).

2.2 *Methods: construction of the biosensor*

A 3-mm-diameter glassy carbon (GC) electrode was first polished with alumina (Al_2O_3) slurry of successively smaller particles (1.0, 0.3, and 0.05 μm diameters). Then, the electrode was cleaned by ultrasonication in ultrapure water and ethanol, successively. In a typical procedure for the preparation of the PAA-$Au_{core}Co_3O_{4shell}$-HRP modified electrode, the $Au_{core}Co_3O_{4shell}$ colloid prepared as previously described[9] was firstly sonicated for 1 h to aid in the dissolution of the $Au_{core}Co_3O_{4shell}$, then equal volumes of pure PAA, 3.75 mg/ml HRP, and $Au_{core}Co_3O_{4shell}$ colloidal solution were mixed. Next, 5 μl of the solution was cast onto the GC electrode surface with a 10-μl syringe. Finally, the modified electrode was left to dry for over 20 h at room temperature. The modified electrode was stored at 4°C in a refrigerator when not in use.

For comparison with the PAA-$Au_{core}Co_3O_{4shell}$-HRP modified electrode, a PAA/$Au_{core}Co_3O_{4shell}$ modified electrode was also prepared using the same procedure described above.

2.3 *Apparatus and measurements*

All electrochemical measurements were performed at room temperature using a CHI 660C electrochemical workstation (CH Instru. Co., Shanghai, China). The measurements were based on a three-electrode system with the as-prepared film electrodes as the working electrodes, a Ag/AgCl (3M KCl) electrode as the reference electrode, and a platinum wire as the auxiliary electrode. A 20 mM pH 7.0 PBS was used as the electrolyte in all the experiments. The buffer solution was deoxygenated by continuous sparging with highly purified nitrogen for at least 30 min before the measurements, and a nitrogen atmosphere environment was maintained in all electrochemical measurements.

Electrochemical impedance spectroscopy (EIS) was carried out in 0.1 M pH 7.0 KCl solution containing 5 mM $[Fe(CN)_6]^{3-/4-}$ (1:1) using an AUTOLAB advanced electrochemical system (Swiss).

UV-visible absorption spectroscopy was carried out with a U-3010 spectrophotometer (Hitachi, Japan) using two 1-cm quartz cells. Sample films for the measurement were prepared by casting PAA, $Au_{core}Co_3O_{4shell}$ colloid, PAA-HRP, and PAA-$Au_{core}Co_3O_{4shell}$-HRP solutions onto quartz glass slides and drying them in air. The thus-obtained dry glass films were examined.

3. Results and Discussion

3.1 *Biocompatibility and electron transfer property characterization of the PAA-$Au_{core}Co_3O_{4shell}$-HRP composite film*

UV-visible absorption is sensitive for determining the characteristic structure of nanomaterials and proteins.[29–31] Previous studies have proved that the biological activity of heme proteins depends on the Soret absorption band position of heme because it can provide information on the possible denaturation of heme proteins.[32,33] Figure 1 shows the UV-visible absorption spectra of HRP solution and the dry PAA, $Au_{core}Co_3O_{4shell}$, PAA-HRP, and PAA-$Au_{core}Co_3O_{4shell}$-HRP films. No UV-visible absorption peaks of the dry PAA or $Au_{core}Co_3O_{4shell}$ film can be observed (curves a and b, respectively). However, characteristic Soret absorption bands at approximately 403 nm can be clearly observed in the UV-visible spectra of the dry HRP-PAA (curve d) and HRP-PAA-$Au_{core}Co_3O_{4shell}$ (curve e) composite films, which are approximately consistent with that of native HRP in pH 7.0 PBS (curve c). These results suggest that PAA and $Au_{core}Co_3O_{4shell}$ could not lower the bioactivity of HRP or HRP trapped in a composite film owing to these compounds having a similar structure to native-state HRP in PBS.

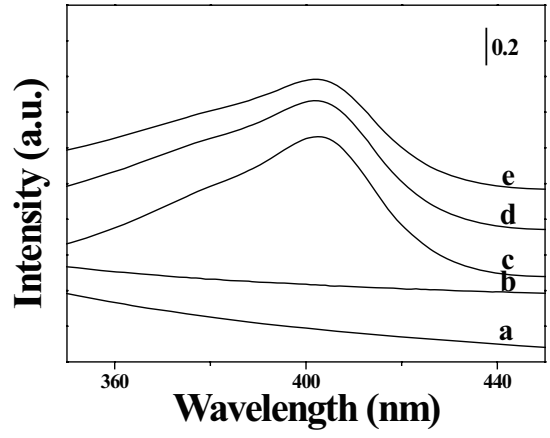

Fig. 1. UV-visible absorption spectra of (a) dry PAA film, (b) dry $Au_{core}Co_3O_{4shell}$ film, (c) HRP solution, (d) dry PAA-HRP composite film, and (e) dry PAA-$Au_{core}Co_3O_{4shell}$-HRP composite film on quartz glass slides.

EIS is a powerful tool for determining the interface properties of surface-modified electrodes.[34] Figure 2 shows the electrochemical impedance spectra (Nyquist plots) of different modified GC electrodes in 0.1 M pH 7.0 KCl solution containing 5 mM $[Fe(CN)_6]^{3-/4-}$ (1:1). In the Nyquist plot of EIS, the semicircle portion at higher frequencies corresponds to an electron-transfer-limited process, and the linear portion at lower frequencies corresponds to a diffusion-controlled process.[35] In the bare GC electrode (curve b), electron transfer resistance (R_{ct}) is about 410 Ω. An obvious decrease in R_{ct} (about 292 Ω) was observed when PAA was immobilized on GC electrode (curve a), indicating that the PAA may pro mote the electron transfer from the redox probe $[Fe(CN)_6]^{3-/4-}$ to the underlying electrode. A marked increase in R_{ct} (about 3000 Ω, curve d) was observed when HRP was immobilized on a GC electrode by cross-linking with PAA, which can be ascribed to the resistance of the macromolecular structure of HRP to electron transfer, and also confirms the successful immobilization of HRP.[36] However, the R_{ct} (about 2400 Ω) at the PAA-$Au_{core}Co_3O_{4shell}$-HRP/GC electrode decreases again (curve c), indicating that $Au_{core}Co_3O_{4shell}$ nanocubes could facilitate electron transfer.

3.2 *Direct electrochemistry of the immobilized HRP*

Figure 3 shows representative cyclic voltammograms of the PAA-$Au_{core}Co_3O_{4shell}$/GC and PAA-$Au_{core}Co_3O_{4shell}$-HRP/GC electrodes in 20 mM PBS at a scan rate of 0.20 V/s. At the PAA-$Au_{core}Co_3O_{4shell}$/GC electrode, no redox peak was observed (curve a), indicating that both PAA and $Au_{core}Co_3O_{4shell}$ do not undergo electrochemical reactions in the potential range studied. However, stable, nearly reversible, and well-defined peaks for HRP-Fe^{III}/Fe^{II} redox couple were observed at the PAA-$Au_{core}Co_3O_{4shell}$-HRP/GC electrode (curve b), which could be ascribed to the direct electron transfer between HRP

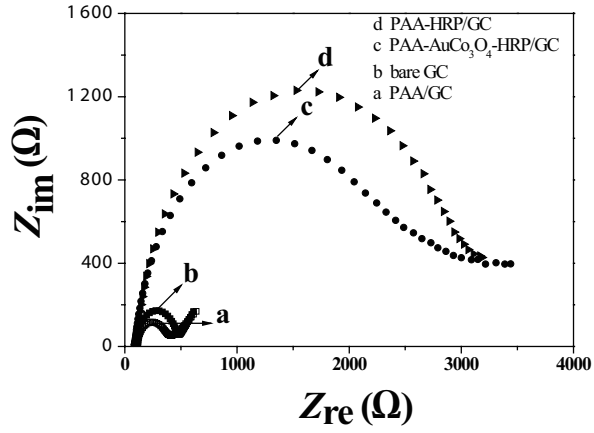

Fig. 2. Nyquist plots of different modified GC electrodes in 5 mM $[Fe(CN)_6]^{3-/4-}$ and 0.1 M KCl solution at pH 7.0: (a) PAA/GC, (b) bare GC, (c) PAA-$Au_{core}Co_3O_{4shell}$-HRP/GC, and (d) PAA-HRP/GC.

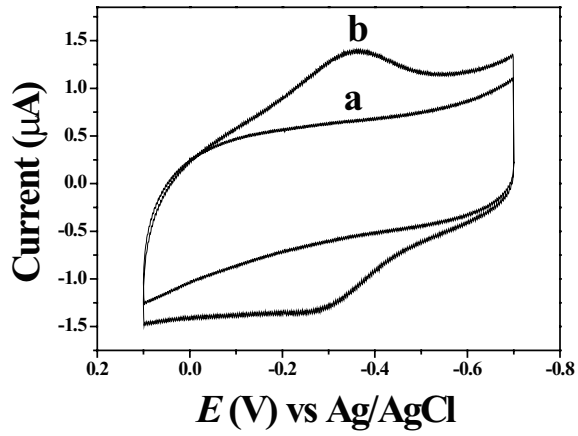

Fig. 3. Cyclic voltammograms of different modified electrodes in 20 mM pH 7.0 PBS: (a) PAA-$Au_{core}Co_3O_{4shell}$/GC and (b) PAA-$Au_{core}Co_3O_{4shell}$-HRP/GC. Scan rate: 0.20 V/s.

and the underlying electrode. The formal potential $E^{\circ\prime}$ (estimated as (Ep,a + Ep,c)/2, where Ep,a and Ep,c are the anodic and cathodic peak potentials, respectively) of HRP is about −0.31 V vs Ag/AgCl, which is similar to those obtained in some previous studies.[37–39] The peak-to-peak separation ΔEp, which is directly related to electron transfer rate, is about 50 mV. Such a small ΔEp reveals a fast and quasi-reversible electron transfer process.

Figure 4 shows typical cyclic voltammograms of the PAA-$Au_{core}Co_3O_{4shell}$-HRP/GC electrode with scan rates from 0.05 to 0.80 V/s. As studied previously,[40] besides an increasing peak separation, both cathodic and anodic peak currents of HRP increase linearly with increasing scan rate, as shown in the inset of Fig. 4; moreover, ΔEp increases with scan rate, indicating that all the electroactive HRP in the film was reduced on the forward cathodic scan and the reduced HRP was then converted to the oxidized form on the reverse anodic scan. This result indicated that the PAA-$Au_{core}Co_3O_{4shell}$ composite film provides a friendly microenvironment for the captured HRP to enable the electron transfer between HRP and the GC electrode and it is a surface-confined electrochemical process. According to Faraday's law ($Q = nFA\Gamma^*$), the average surface concentration of electroactive HRP (Γ^*) in the PAA-HRP film is about 6.80×10^{-11} mol/cm^2 (assuming a one-electron transfer reaction), which is about 2 times higher than that of HRP in chitosan and approximately 3 times higher than that of the theoretical monolayer coverage.[41] This result indicates that multilayers of HRP entrapped in the as-prepared film share in the electron-transfer process.

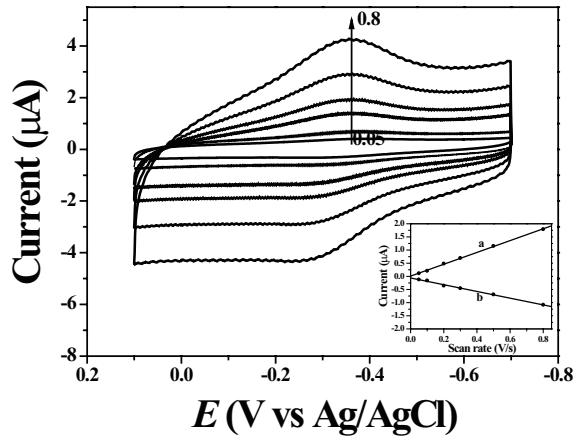

Fig. 4. Cyclic voltammograms of PAA-$Au_{core}Co_3O_{4shell}$-HRP modified electrode measured at scan rates of 0.05, 0.10, 0.20, 0.30, 0.50, and 0.80 V/s. Inset: calibration plot of cathodic (curve a) and anodic (curve b) peak currents vs scan rate.

The kinetic parameter k_s was estimated using the model of Laviron:[42]

$$\log k_s/s^{-1} = \alpha \log (1-\alpha) + (1-\alpha) \log \alpha - \log \left[\left(\frac{RT}{nF\upsilon} \right) \Big/ s \right] - \frac{\alpha(1-\alpha)nF\Delta Ep}{2.3RT}, \quad (1)$$

where α is the charge transfer coefficient, k_s is the heterogeneous electron transfer rate constant, ΔEp is the peak separation, n is the number of electrons transferred in the rate-determining reaction, R is the gas constant, T is the absolute temperature, and υ is the scan rate. According to the method of Laviron, taking charge transfer α to be 0.5 and scan rate to be 0.8 V/s with ΔEp 75 mV, the k_s of HRP is calculated to be 7.4 s^{-1}, suggesting a fast electron transfer process.

3.3 *Electrocatalytic reduction of H_2O_2*

HRP immobilized on an electrode surface usually has excellent electrocatalytic activity towards H_2O_2.[24] Figure 5 shows the electrocatalytic properties of H_2O_2 solutions of different concentrations at the PAA-$Au_{core}Co_3O_{4shell}$-HRP/GC electrode. The cathodic peak current at approximately −0.35 V (vs Ag/AgCl) apparently increases, whereas its corresponding anodic peak current decreases as H_2O_2 is successively added to PBS, suggesting a representative electrocatalytic reduction of H_2O_2. Moreover, the cathodic peak current increases linearly within a certain range of H_2O_2 concentrations (inset of Fig. 5), indicating that HRP immobilized in a PAA-$Au_{core}Co_3O_{4shell}$-HRP composite film has good bioelectrocatalytic activities towards H_2O_2. The possible mechanism of the

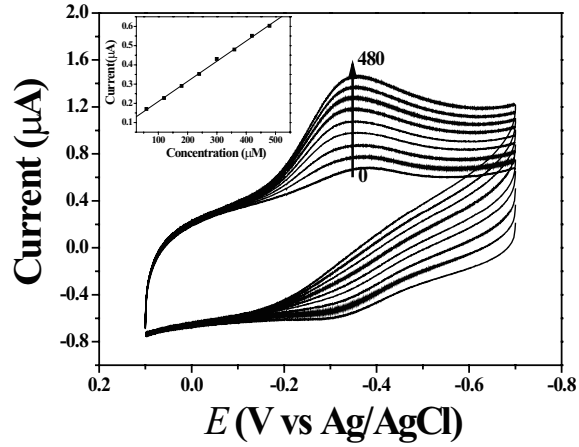

Fig. 5. Electrocatalysis of PAA-$Au_{core}Co_3O_{4shell}$-HRP/GC electrode towards H_2O_2 in 20 mM pH 7.0 PBS at scan rate 0.1 V/s. H_2O_2 concentrations of 0, 60, 120, 180, 240, 300, 360, 420, and 480 μM successively increased from bottom to top. Inset: calibration curve of cathodic peak current vs H_2O_2 concentration (R = 0.9993).

electrocatalytic reduction of H_2O_2 at the HRP-based enzyme electrode should be similar to that reported recently, which can be expressed as follows:[43]

$$\text{HRP[Heme(Fe}^{\text{III}}\text{)]} + H_2O_2 \rightarrow \text{Compound I} + H_2O \quad (2)$$

$$\text{Compound I} + H_2O_2 \rightarrow \text{HRP[Heme(Fe}^{\text{III}}\text{)]} + H_2O + O_2 \quad (3)$$

$$\text{HRP[Heme(Fe}^{\text{III}}\text{)]} + H^+ + e^- \rightarrow \text{HRP[Heme(Fe}^{\text{II}}\text{)]} \quad \text{at electrode} \quad (4)$$

$$\text{HRP[Heme(Fe}^{\text{II}}\text{)]} + O_2 \rightarrow \text{HRP[Heme(Fe}^{\text{II}}\text{)]-}O_2 \quad \text{fast} \quad (5)$$

$$\text{HRP[Heme(Fe}^{\text{II}}\text{)]-}O_2 + H^+ + e^- \rightarrow \text{HRP[Heme(Fe}^{\text{III}}\text{)]} + H_2O_2 \quad \text{at electrode} \quad (6)$$

The overall reaction of (1)–(5) would be

$$H_2O_2 + 2H^+ + 2e^- \rightarrow 2H_2O. \quad (7)$$

Figure 6 shows a plot of the variation in electrocatalytic current (I_{cat}) against H_2O_2 concentration for the PAA-$Au_{core}Co_3O_{4shell}$-HRP/GC electrode in 20 mM pH 7.0 PBS. Along with increasing H_2O_2 concentration from 2 to 370 μM, I_{cat} linearly increases, indicating that the linear range is from 2.0×10^{-6} to 3.7×10^{-4} M (R = 0.9991, n = 10). The detection limit of H_2O_2 at the PAA-$Au_{core}Co_3O_{4shell}$-HRP electrode is about 9.0×10^{-7} M

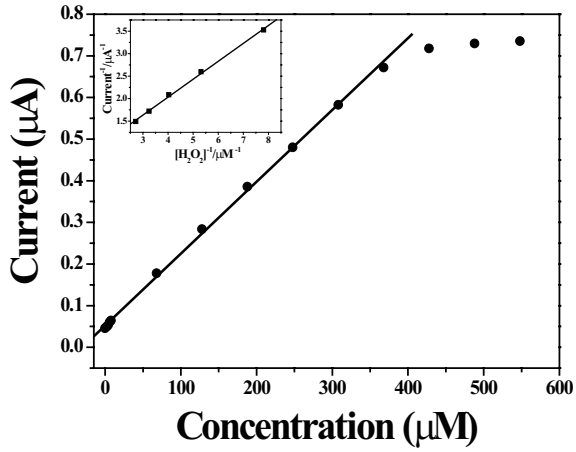

Fig. 6. Plot of variation in electrocatalytic current (I_{cat}) vs H_2O_2 concentration at PAA-$Au_{core}Co_3O_{4shell}$-HRP/GC electrode in 20 mM pH 7.0 PBS at scan rate of 0.1 V/s. Inset: relative Lineweaver-Burk plot (R = 0.9991, n = 10).

when the signal-to-noise ratio (S/N) is 3. However, when higher H_2O_2 concentrations were added, the plot tends to level off, showing a typical Michaelis-Menton process. According to the Lineweaver-Burk equation,[44]

$$I_{SS}^{-1} = I_{max}^{-1} + K_M c^{-1} I_{max}^{-1} , \tag{8}$$

where I_{ss} is the catalytic current, c is the bulk concentration of the substrate, I_{max} is the maximum catalytic current, and K_M is the Michaelis constant. Herein, the Lineweaver-Burk plot gives a K_M of 0.91 mM for the PAA-$Au_{core}Co_3O_{4shell}$-HRP electrode (inset in Fig. 6). The small K_M indicates that the PAA-$Au_{core}Co_3O_{4shell}$-HRP electrode has a high catalytic efficiency for the reduction of H_2O_2 over a wide linear range.

To further study the performance of the biosensor, the amperometric response of the as-prepared biosensor for H_2O_2 was also investigated by amperometric current-time curve method. On the basis of the optimal experiments, a constant potential of −0.35 V was selected as the applied potential for high sensitivity. Figure 7 shows a typical current-time curve of the biosensor (PAA-$Au_{core}Co_3O_{4shell}$-HRP/GC electrode) for 6, 10, and 20 μM H_2O_2 solutions added successively to pH 7.0 PBS. With a stepwise increase in H_2O_2 concentration in the stirred PBS, the biosensor responded rapidly to the substrate and a stepwise growth in reduction current was observed. The response time of about 2 s (achieving 95% of the steady-state current) indicates a fast process and the immobilized HRP could catalyze H_2O_2 well. Such a fast response can be ascribed to the fast diffusion of the substrate in the composite film.

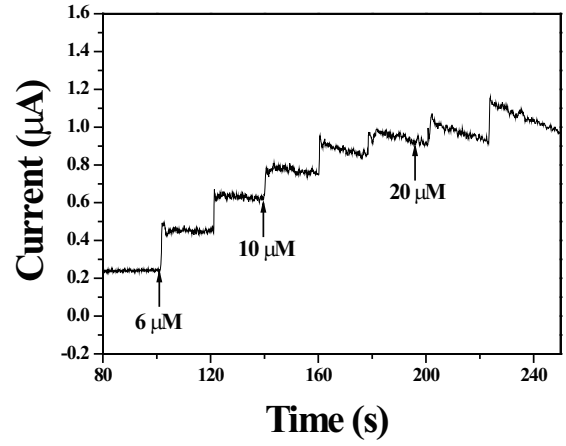

Fig. 7. Typical current-time response curve of the PAA-$Au_{core}Co_3O_{4shell}$-HRP biosensor upon successive addition of 6, 10, and 20 μM H_2O_2 solutions to pH 7.0 PBS at applied potential of −0.35 V (vs Ag/AgCl).

3.4 *Stability and reproducibility of the PAA-$Au_{core}Co_3O_{4shell}$-HRP composite film*

To widen the range of biosensor applications, besides high sensitivity and good biological activity, reproducibility and stability are of key importance for a biosensor. When the PAA-$Au_{core}Co_3O_{4shell}$-HRP/GC electrode was used to successively scan 15 circles at a scan rate of 0.20 V/s, no obvious changes appear in the cyclic voltammograms. The relative standard deviation (R.S.D.) of the biosensor produced is 0.91% for 15 successive measurements, suggesting that the biosensor has excellent reproducibility.

HRP biosensor stability can be evaluated by measuring the cyclic voltammetric peak current of HRP at long-term time intervals. The biosensor was stored under dry condition at 4°C when it was not in use. The decrease in cathodic peak current is less than 2.0% after 40 days, indicating that the as-prepared biosensor has good long-term stability. This stability could be attributed to the excellent biocompatibility and favorable microenvironment of the sensor for HRP to retain its bioactivity.

4. Conclusions

In summary, we have designed a novel biosensor composed of PAA, HRP, and $Au_{core}Co_3O_{4shell}$ composite film. The method we used may be extendable to the preparation of other biosensors constructed with polymers, nanomaterials, and redox-protein molecules. Our results demonstrate that HRP effectively retains its native structure in PAA-$Au_{core}Co_3O_{4shell}$-HRP composite films, at which direct electron transfer and electrocatalytic activity could be effectively achieved. Also, the as-prepared biosensor was demonstrated to possess multilayer coverage and exhibit good

reproducibility, stability, fast response, and excellent biological activity. For example, the biosensor has a fast amperometric response (about 2 s) to H_2O_2 with a linear range of 2.0×10^{-6} to 3.7×10^{-4} M, and has a k_s and a K_M of about 7.4 s^{-1} and 0.91 mM, respectively. The unique polymer-nanomaterial composite materials used are expected to offer a good biosensing platform for other redox proteins and to find applications in biosensing, biocatalysis, and biodetection.

Acknowledgements

The work was supported by the National Natural Science Foundation of China (No. 20773040), The Research Fund for the Doctoral Program (New Young Teacher) of Higher Education (No. 20070561005), Natural Science Foundation of Guangdong Province (No. 07006555), and One Hundred Person Project of The South China University of Technology.

References

1 J. Wang: Chem. Rev. **108** (2008) 814.
2 G. Z. Liu, M. N. Paddon-Row and J. J. Gooding: Electrochem. Commun. **9** (2007) 2218.
3 X. H. Chen, J. Q. Hu, Z. W. Chen, X. M. Feng and A. Q. Li: Biosens. Bioelectron. **24** (2009) 3448.
4 Z. H. Dai, K. Liu, Y. W. Tang, X. D. Yang, J. C. Bao and J. Shen: J. Mater. Chem. **18** (2008) 1919.
5 D. Ivnitski, K. Artyushkova, R. A. Rincón, P. Atanassov, H. R. Luckarift and G. R. Johnson: Small **3** (2008) 357.
6 O. Niwa, D. Kato, R. Kurita, T. You, Y. Iwasaki and S. Hirono: Sens. Mater. **19** (2007) 225.
7 Z. W. Chen, Y. Yu, H. Guo and J. Q. Hu: J. Phys. D Appl. Phys. **42** (2009) 125307.
8 W. L. Shi, H. Zeng, Y. Sahoo, T. Y. Ohulchanskyy, Y. Ding, Z. L. Wang, M. Swihart and P. N. Prasad: Nano Lett. **6** (2006) 875.
9 J. Q. Hu, Z. H. Wen, Q. Wang, X. Yao, Q. Zhang, J. H. Zhou and J. H. Li: J. Phys. Chem. B **110** (2006) 24305.
10 M. A. Langell, M. D. Anderson, G. A. Carson, L. Peng and S. Smith: Phys. Rev. B **59** (1999) 4791.
11 X. Wang, X. Y. Chen, L. S. Gao, H. G. Zheng, Z. Zhang and Y. T. Qian: J. Phys. Chem. B **108** (2004) 16401.
12 D. A. Resnick, K. Gilmore, Y. U. Idzerda, M. T. Klem, M. Allen, T. Douglas, E. Arenholz and M. Young: J. Appl. Phys. **99** (2006) 08Q501.
13 L. P. Zhou, J. Xu, H. Miao, F. Wang and X. Q. Li: Appl. Catal. A: Gen. **292** (2005) 223.
14 R. M. Wang, C. M. Liu, H. Z. Zhang, C. P. Chen, L. Guo, H. B. Xu and S. H. Yang: Appl. Phys. Lett. **85** (2004) 2080.
15 T. He, D. Chen, X. Jiao and Y. Wang: Adv. Mater. **18** (2006) 1078.
16 J. Feng and H. C. Zeng: Chem. Mater. **15** (2003) 2829.
17 Y. S. Ding, L. P. Xu, C. H. Chen, X. F. Shen and S. L. Suib: J. Phys. Chem. C **112** (2008) 8177.
18 M. M. Natile and A. Glisenti: Chem. Mater. **15** (2003) 2502.
19 Y. D. Meng, D. R. Chen and X. L. Jiao: J. Phys. Chem. B **110** (2006) 15212.
20 Y. Tak and K. Yong: J. Phys. Chem. C **112** (2008) 74.

21 X. B. Lu, G. F. Zou and J. H. Li: J. Mater. Chem. **17** (2007) 1427.
22 K. M. Bromley, A. J. Patil, A. M. Seddon, P. Booth and S. Mann: Adv. Mater. **19** (2007) 2433.
23 Y. Iwasaki, O. Niwa and M. Morita: Sens. Mater. **11** (1999) 51.
24 Y. Fujimori, Y. Gotoh, N. Tamaki, Y. Ohkoshi and M. Nagura: J. Mater. Chem. **15** (2005) 4816.
25 A. Glidle, T. Yasukawa, C. S. Hadyoon, N. Anicet, T. Matsue, M. Nomura and J. M. Cooper: Anal. Chem. **75** (2003) 2559.
26 B. Z. Wang, J. Anzai, W. L. Gong, M. Q. Wang and X. Y. Du: Sens. Mater. **20** (2008) 221.
27 O. A. Raitman, E. Katz, A. F. Buckmann and I. Willner: J. Am. Chem. Soc. **124** (2002) 6487.
28 A. K. M. Kafi, D. Y. Lee, S. H. Park and Y. S. Kwon: Thin Solid Films **515** (2007) 5179.
29 J. Q. Hu, Q. Chen, Z. X. Xie, G. B. Han, R. H. Wang, B. Ren, Y. Zhang, Z. L. Yang and Z. Q. Tian: Adv. Funct. Mater. **14** (2004) 183.
30 J. Q. Hu, Y. Zhang, B. Liu, J. X. Liu, H. H. Zhou, Y. F. Xu, Y. X. Jiang, Z. L. Yang and Z. Q. Tian: J. Am. Chem. Soc. **126** (2004) 9470.
31 L. Zhang, Q. Zhang and J. H. Li: Adv. Funct. Mater. **17** (2007) 1958.
32 H. Huang, N. F. Hu, Y. H. Zeng and G. Zhou: Anal. Biochem. **308** (2002) 141.
33 H. Theorell and V. Ehrenberg: Acta. Chem. Scand. **5** (1951) 823.
34 J. T. Zhu, C. G. Shi, J. J. Xu and H. Y. Chen: Bioelectrochem. **71** (2007) 243.
35 R. J. Pei, Z. L. Cheng, E. K. Wang and X. R. Yang: Biosens. Bioelectron. **16** (2001) 355.
36 X. L. Luo, J. J. Xu, Q. Zhang, G. J. Yang and H. Y. Chen: Biosens. Bioelectron. **21** (2005) 190.
37 H. J. Chen and S. J. Dong: Biosens. Bioelectron. **22** (2007) 1811.
38 S. F. Wang, T. Chen, Z. L. Zhang, X. C. Shen, Z. X. Lu, D. W. Pang and K. Y. Wong: Langmuir **21** (2005) 9260.
39 Y. L. Zhou, N. F. Hu, Y. H. Zeng and J. F. Rusling: Langmuir **18** (2002) 211.
40 X. B. Lu, Z. H. Wen and J. H. Li: Biomaterials **27** (2006) 5740.
41 H. Huang, N. F. Hu, Y. H. Zeng and G. Zhou: Anal. Biochem. **308** (2002) 141.
42 E. Laviron: J. Electroanal. Chem. **101** (1979) 19.
43 X. B. Lu, H. J. Zhang, Y. W. Ni, Q. Zhang and J. P. Chen: Biosens. Bioelectron. **24** (2008) 93.
44 R. A. Kamin and G. S. Wilson: Anal. Chem. **52** (1980) 1198.